ROYAL SOCIETY
OF CHEMISTRY

PAPER

Nanoengineering ABO₃ active sites from low-energy routes (TX100-stabilised water-in-oil microemulsions, surface segregation and surface complexation on colloidal AlOOH/sol–gel Al₂O₃ surfaces) for pollution control catalysis

M. P. Worsley,[a] P. N. Forrest,[b] S. Roesch,[b] C. Thatcher,[b] P. A. Sermon*[a] and P. Kaur[c]

It is shown that water-in-oil microemulsions (*m/e* or μE) can produce $BaCeO_3$ (BCO) and $LaCoO_3$ (LCO) precursors. The nanoparticles (NPs) adsorb on AlOOH sols, in much the same way as Turkevich previously immobilised platinum group metal sols. BCO is active in CO and propane oxidation and NO removal under stoichiometric exhaust conditions, but LCO is a better oxidation catalyst. Activity was also seen when Ba,Ce and La,Co are inserted into/segregate at the surface of $AlOOH/Al_2O_3$. However, there is only formation of low levels of BCO, $CAlO_3$ (CAO), LCO and $LaAlO_3$ (LAO) perovskites, along with aluminates and separate oxides. The complexing of cations by AlOOH surface-held oxalate ions, albeit with different efficiencies, has also been explored. All three routes yield active catalysts with micro-domains of crystallinity; microemulsions produce the best defined perovskite NPs, but even those from surface segregation have higher turnover numbers than traditional Pt catalysts. Perovskite NPs may open up green chemistry for air pollution control that is consistent with a circular economy.

1. Introduction

The authors were intrigued by Turkevich's historic reports of adsorbing and supporting precious metal colloidal particles on AlOOH boehmite,[1] taking advantage of electrostatic attraction, after which transmission electron microscopy (TEM) characterised the surface-held discrete NPs and in parallel catalytic

[a]*Nanomaterials Laboratory, Wolfson Centre, Brunel University, Uxbridge, Middx., UB8 3PH, UK. E-mail: paul.sermon@brunel.ac.uk*

[b]*Department of Chemistry, University of Surrey, Guildford, GU2 7XH, UK*

[c]*Horiba MIRA Ltd, Nuneaton, CV10 0TU, UK*
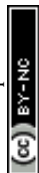
activity could be measured directly. They wanted to see whether the approach might be applied to perovskites.[2]

Routes to perovskites can be high-[3] and low-temperature/energy[4–8] (e.g. sol–gel, microwave-assisted sol–gel, electrospinning, hydrothermal synthesis, micro-emulsion) and mechanochemical.[9] Some offer opportunities to prepare nano-particles (NPs; d < 100 nm) with different structures: ultrasonics,[10] microwaves (MW)[11] and chelators (oxalic acid,[12] citric acid[13] and tartrate[14]), sometimes in one-step preparations.[15] Oxide, halide and oxyhalide perovskite[16] nanoparticles (NPs) can all be produced by such routes. They are used in a wide range of applications:[17–33] (i) photovoltaic solar cells, (ii) LEDs, photoelectrodes, battery anodes, H_2O and CO_2 electrochemistry, (iii) photocatalysis, (iv) catalysis (e.g. combustion of pollutant soot particles with MW regeneration, water gas shift, toluene oxidation, CO methanation and CO oxidation (where activity can be MW-enhanced)), (v) gas sensing, (vi) dielectric heating, (vii) magnetotransport and (viii) biomedicine (e.g. hyperthermia and drug delivery). In all these areas perovskite NPs are especially advantageous[34] and may be enhanced further by zero-valent NPs,[35] supports[36] or templates (both inorganic[37] or polymeric[38]).

Green catalytic chemistry and resource efficiency are at the heart of a minimum waste circular economy.[39] It has long been thought that ABO_3 perovskites[40] had an advantage in a circular economy over precious metals, provided that their surface areas could be raised above a very modest 1.4 m^2 g^{-1} (ref. 41) as reported by Libby, celebrated for his work on 14C radiocarbon dating, and this might be helped by supporting[36] or incorporating a polymer or Al_2O_3.

Previously some of the present authors have attempted to nanoengineer catalysts: (a) produced colloidal Pt_xAu_{1-x}Au and Pt–SnO_y alloy sols that were adsorbed on carbon or Al_2O_3 surfaces,[42] (b) synthesised[43] sol–gel Pt–Sn–K/SiO_2–Al_2O_3 hydro-carbon conversion catalysts containing $K_2Pt(OH)_6$ perovskite precursors[44] and (c) taken $[AlO_4Al_{12}(OH)_{24}(H_2O)_{12}]^{7+}$ Keggin ions (whose formation was followed by ^{27}Al solution NMR in terms of 4-coordinate AlO_4 at about 60 ppm and 6-coordinate AlO_6 at about 2.5 ppm as a function of prevailing OH^-/Al^{3+} ratios) and partially replaced Al^{3+} with Fe^{3+} or Au^{3+} (ref. 45). These were adsorbed to a 5% loading on SiO_2 surfaces. They showed a similar light-off temperature (LOT) for CO oxidation (870 K) to commercial platinum-group metal three-way catalysts (TWCs) (812 K) in a stoichio-metric gas stream. Maximum% conversion of CO at 633 K was seen at Au : Fe = 25 : 75, but these were thermally unstable.

Now we have investigated whether the $BaCeO_3$ (BCO) and $LaAl_{1-x}Co_xO_3$ (LACO) perovskite active sites and the sol–gel host could be designed simulta-neously to form intriguing environmental catalysts by:

(i) forming these as NPs in aqueous droplets in water-in-oil microemulsions and harvesting by a phase inversion step at 273 K (appreciating that these might be unstable during calcination),

(ii) causing them to form at the surface of colloidal AlOOH or sol–gel Al_2O_3 as the component concentrations were progressively raised beyond the point of maximum solubility in the supporting sol–gel matrix. Alumina was chosen because it is a frequent catalyst support that comes in γ, δ and θ forms.[46] In the latter, nanowires can be seen in high resolution TEM (HRTEM). Boehmite AlOOH converts to γ-alumina at 723 K, then δ, then θ and finally the α-phase at 1473 K. It can form a defective cubic O^{2-} close-packing spinel structure with 16 possible octahedral sites and 8 tetrahedral sites for Al^{3+} and other stabilising cations. One

knows that there is a maximum solubility of such stabilising cations (La^{3+}/Fe^{2+}, Ba^{2+}/Ce^{4+}, and La^{3+}/Co^{2+}, *etc.*) beyond which phases are formed at the alumina surface. Alumina can be stabilised by $Ce^{3+/4+}$ or Ba^{2+};[47] the authors appreciated that dispersed CeO_2 NPs (including octapods[48]) could be formed and M^{x+}-alumina reactions could produce spinel $BaAl_2O_4$,[49] barium hexaluminates, $Ce^{3+/4+}AlO_y$ phases[50] or perovskite $CeAlO_3$ (CAO)[51] phases, and

(iii) adsorbing oxalate ions on the surface of peptized AlOOH needles and reacting these with the perovskite cations in aqueous solution to give an insoluble surface oxalate that decomposes on calcination.

Goldschmidt[46] in the 1920s explored ABX_3 perovskites. Orthorhombic BCO forms at 1170–1223 K (ref. 52) and $LaFeO_3$ (LFeO) exhibited its most intense {002} X-ray reflections[53] at $2\theta = 28.68°$ and $2\theta = 32.20°$. Rhombohedral LCO prepared at 1013 K (ref. 54 and 55) has its most intense {110} and {104} reflections at $2\theta = 34°$.[56] But HRTEM is useful in detecting nanoscale perovskite domains (*e.g.* in LCO[57]). Surface titrations (COT_O–OT_{CO})[58] help probe active sites and oxygen-storage capacity (OSC)[59] that may be introduced by CeO_2 (ref. 60 and 61) or Tb_4O_7–CeO_2,[62,63] sometimes promoted by platinum-group metals.[64] Here it is perovskite nanoparticles that are characterised by X-ray diffraction (XRD), Raman, HRTEM, UV/vis, temperature-programmed reduction/oxidation (TPR/TPO) and XPS. It is important that these methods differentiate perovskite NP phases from other by-product phases (*e.g.* aluminates[65]). After characterising these they were evaluated for CO (and hydrocarbon) oxidation (where rates might be different on different facets[66]). 28–118 nm $LaAl_{1-x}Mn_xO_3$ (LAMnO) and $LaAl_{1-x}Fe_xO_3$ (LAFeO) perovskites are good catalysts.[67,68] Cu-doped $LaAlO_3$ (LAO)[69] and $LaCoO_3$ (LCO)[70] are photocatalysts and electrochemically active.[71] Partial Pd-replacement of Al^{3+} in LAO produces three-way catalytic (TWC) activity in vehicle exhaust conditions.[72] LCO and LAO are formed at higher La and Co loadings in sol–gel alumina[73] (where some say that LAO is an inert perovskite, but others suggest citrate-derived LAO is active in the oxidative-coupling of methane (OCM)[74]), but 42.2 nm La_2CoAlO_6 double perovskite is more active and has a lower light-off temperature (LOT; 707.1 K) in CH_4 catalysed combustion[75] than either LCO (763.6 K) or LAO (845.3 K).

2. Experimental

AlOOH synthesis

0.236 g AlOOH was prepared in 100 cm^3 distilled H_2O (initially at 353–358 K) by adding 3.9 mmol aluminium-tri-*sec*-butoxide (ASB, Aldrich, 97%), raising the reflux temperature to 403–413 K, adding 3.9 mmol HCl and refluxing for 48 h to reach a pH of 3.1. One fraction of this AlOOH dispersion was used directly; another was freeze-dried to an AlOOH powder that was calcined at 773 K and then 923 K. Dynamic light scattering (DLS) showed that the average particle size of the AlOOH sol was 60 nm (Fig. 1c); as this was calcined to higher temperatures it would inevitably transform ($\gamma \rightarrow \delta \rightarrow \theta \rightarrow \alpha$).[46]

BCO and LCO synthesis by phase inversion at 273 K in a TX100-stabilised water-in-oil microemulsion

Here two homogenous 0.2 M TX100-stabilised water-in-cyclohexane (90%)/2-methyl-2-propanol (10%) microemulsions were used. In one µE a slight excess of
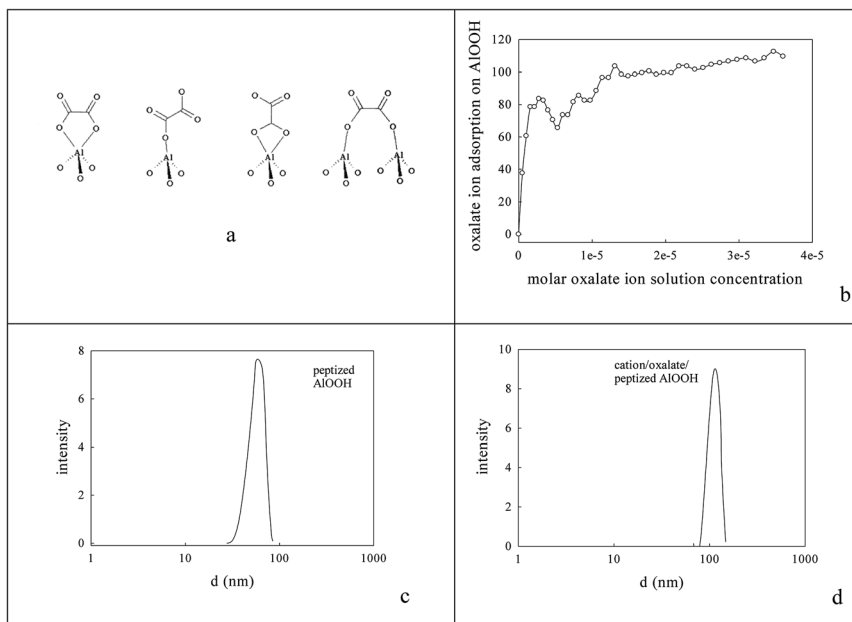
Fig. 1 Nature of oxalate anion adsorption on AlOOH[8,85] (a, b). DLS estimate of the average particle size in aqueous dispersions of (c) the peptized AlOOH (60 nm) and (d) after oxalate adsorption and formation of 3.65% cation/oxalate/AlOOH (114 nm).

ammonium oxalate was introduced to the dispersed water droplets. In another μE mixed 0.02 M La,Co nitrates (or mixed 0.02 M Ba,Ce nitrates) were introduced to the dispersed water droplets.[76] The two w/o μEs at 298 K were then mixed to produce (as a result of droplet coalescence/re-dispersion mixed 5–10 nm (defined by the diameter of the aqueous droplet size)) Ba–Ce or La–Co oxalate nano-particles (NPs). The combined microemulsion was then mixed with 50 cm³ of the pre-prepared AlOOH suspension to give Ba–Ce oxalate/AlOOH or La–Co oxalate/AlOOH that were harvested by lowering the combined μE to 273 K (defined by component melting points (280 K, 279.5 K, 273 K and 298–299 K for TX100, cyclohexane, water and 2-methyl-2-propanol)), when two phases appeared. The NP product was found in the upper organic phase. NPs adsorbed on AlOOH, were harvested, washed, dried and calcined (900 K).

Surface segregation using AlOOH/Al$_2$O$_3$, Ce–AlOOH/Al$_2$O$_3$ and Ba,Ce–AlOOH/Al$_2$O$_3$

Surface segregation was attempted using dispersed colloidal AlOOH, where mixed metal cation pairs (Ba^{2+},Ce^{4+} or La^{3+},Co^{3+}) were present in the AlOOH forming/peptizing solution/suspension sufficient to cause 25% Ba,Ce–AlOOH/Al$_2$O$_3$ and 25% La,Co–AlOOH/Al$_2$O$_3$ to form after calcination at 1173 K. Sol–gel–AlOOH/Al$_2$O$_3$ derived Ce- and Ba,Ce-containing catalysts[77,78] were prepared from ASB, 2-methylpentane-2,4-diol (MPD, Aldrich, 99%), Ba(NO$_3$)$_2$–Ce(NO$_3$)$_3$ (Aldrich, 99.999%; dissolved in MPD) and deionised H$_2$O[78,79] as reported previously.[45] For Ba,Ce–AlOOH/Al$_2$O$_3$ the Ba and Ce nitrates were dissolved in MPD at 360 K, followed by ASB and refluxing at 393 K for 6 h under N$_2$. After cooling to 363 K, H$_2$O

was added dropwise over 25 min and refluxing was continued (2 h), followed by ageing at 373 K for 7 days, vacuum-drying (353 K) and then calcining (1173 K; 2 h; static air). Citrates, tartrates or acetates[80,81] could have been used but nitrates were preferred. MPD was both a solvent[82,83] and complexing agent[80]/pore templating agent. Fuentes[83] derived La_2O_3–Al_2O_3 using MPD; here the metal : MPD : H_2O ratio was 1 : 5 : 25. Sol–gel $AlOOH/Al_2O_3$ (BET surface area 179 m^2 g^{-1}) had a higher surface area than when Ce was added (e.g. 16.6% (ICP-MS derived) Ce–$AlOOH/Al_2O_3$ (BET surface area 168 m^2 g^{-1})).

Surface complexation

The peptized AlOOH dispersion had a final pH of 3.1 (below its isoelectric point/point of zero charge (7.8–8.6)) and so it adsorbed oxalate anions[84] on its surface e.g. see Fig. 1a and b; the % adsorption was deduced from the % differential change in suspension conductivity (100% $\times$ $(\sigma_{H_2O} - \sigma_{AlOOH(aq)})/\sigma_{H_2O}$) on sequential addition of 1 cm^3 portions of 10 mM oxalic acid to 50 cm^3 H_2O or $AlOOH_{(aq)}$ respectively). After Ba^{2+},Ce^{4+} or La^{3+},Co^{3+} addition the average DLS particle size rose, almost doubling to 114 nm (Fig. 1c and d). This pre-adsorbed oxalate was titrated with Ba^{2+},Ce^{4+} or La^{3+},Co^{3+} forming a surface layer of low solubility mixed oxalates[84] at an intended 5% loading. However, XPS (using Ba (780.7 eV), Ce (897.7 eV), La (834.7 eV) and Co (781.6 eV) peaks) and FAAS suggested that only a 3.65% metal loading on the oxalate/AlOOH was achieved with Ba : Ce and La : Co ratios on oxalate/AlOOH of 25 : 75 and 30 : 70. This was equivalent to the formation of 0.91% Ba, 2.74% Ce–$AlOOH/Al_2O_3$ and 1.095% La, 2.56% Co–$AlOOH/Al_2O_3$.

Characterization

Malvern DLS, Jeol HRTEM, X'Pert Pro XRD, Supra SEM-EDX and XPS characterization was carried out. TPR,[85] titration and catalysis was followed as now described. Setaram and Thermo Scientific DSC profiles were used for CO (40 μmol) and O_2 (47 μmol) titrations of catalysts in a flowing N_2 (50 cm^3 min^{-1}) inert gas stream held isothermally at a selected temperature. Catalytic measurements were carried out as described previously.[59] Samples (200 mg) were placed in a silica reactor (6 mm diameter) and heated in flowing N_2 to 773 K for 20 min. Then after cooling to 298 K the stoichiometric reactant stream (NO + O_2 oxidant/CO + propane reductant (R) ratio = 1.13, where the reactant stream contained 1000 ppm NO, 5890 ppm O_2, 6000 ppm CO, 520 ppm propane, 10% CO_2 in a N_2 balance) was introduced at 500 cm^3 min^{-1} (equivalent to a 60 000 h^{-1} space velocity in a gasoline-fuelled engine exhaust) at 101 kPa under Brooks smart 5850S mass flow controllers. NDIR, FID-GC and CLD analysers were used for CO/CO_2, propane and NO_x concentrations in real time during heating from 300 K to 900 K at 10 K min^{-1}.

3.   Results

BCO and LCO microemulsion precipitation

Fig. 2a shows the effect of the water content of TX100-stabilised water-in-cyclohexane/2-methyl-2-propanol μE on the partitioning of the surfactant between the water and hydrocarbon phases. There is continuous coalescence and
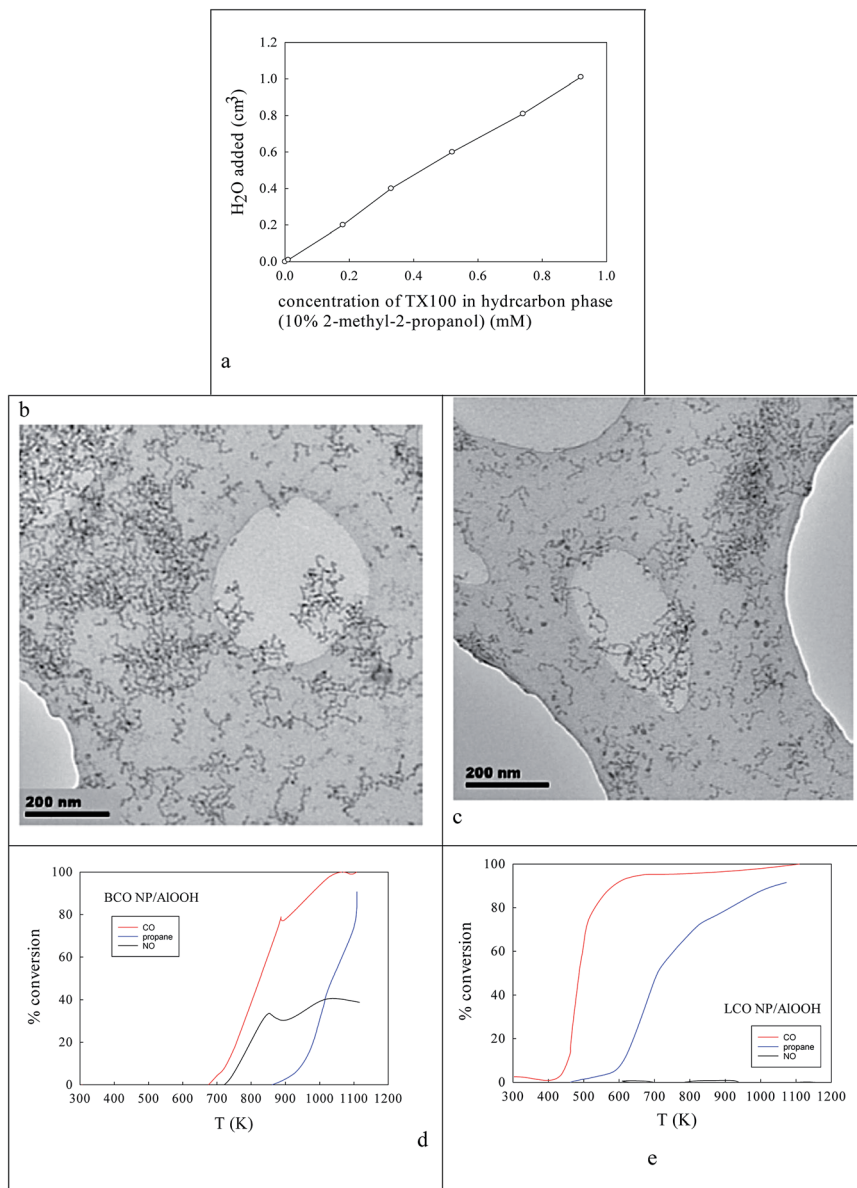
Fig. 2 (a) Effect of H_2O content on TX100 in the oil phase of a H_2O-in-cyclohexane/2-methyl-2-propanol m/z. (b, c) TEM of m/z-derived BCO and LCO NPs and fractal aggregates. (d, e) The activity of such NPs adsorbed onto AlOOH.

separation of nm-sized water droplets, some containing a slight excess of ammonium oxalate and some metal cations. Fig. 2b and c show TEM evidence of the sizes of microemulsion-derived 10–20 nm BCO NPs (with 40–121 nm fractal nanothreads) and 10–21 nm LCO NPs (with and 43–108 nm fractal nano-chains) after phase inversion at 273 K. In Fig. 2d and e one sees the activity of such AlOOH-supported perovskite NPs under stoichiometric conditions as a function

of temperature. Clearly BCO has activity in CO and propane oxidation and more surprisingly in NO conversion (under stoichiometric conditions), but LCO has higher CO and propane activity, but no NO reduction activity. This is promising.

Ba,Ce and La,Co surface segregation[59] on $AlOOH/Al_2O_3$

Clearly the ionic radius of $Ce^{4+/3+}$ (87/101 pm) relative to O^{2-} and Al^{3+} in part defines its solubility in $AlOOH/Al_2O_3$. Fig. 3 shows some characterization data before and after introduction of 20% Ce to the $AlOOH/Al_2O_3$. The sample surface area dropped by 6.1% on this Ce introduction, but HRTEM (Fig. 3a) saw 5 nm nano-crystallites with lattice spacings of 0.19 nm. XRD found after calcination the presence of θ-Al_2O_3, low levels of 10–12 nm γ-Al_2O_3 and CeO_2, but there was no evidence of CAO. Interestingly, in H_2-TPR a 720 K peak (α; H/CeO_2 ratio = 0.156) was associated with alumina-dispersed CeO_2,[85,86] while a 900 K + (β) peak was thought to relate to CAO[88] (that was too fine to be seen XRD) or Ce_2O_3. Fig. 3c shows that CeO_2 addition raises the activity in CO conversion modestly above that
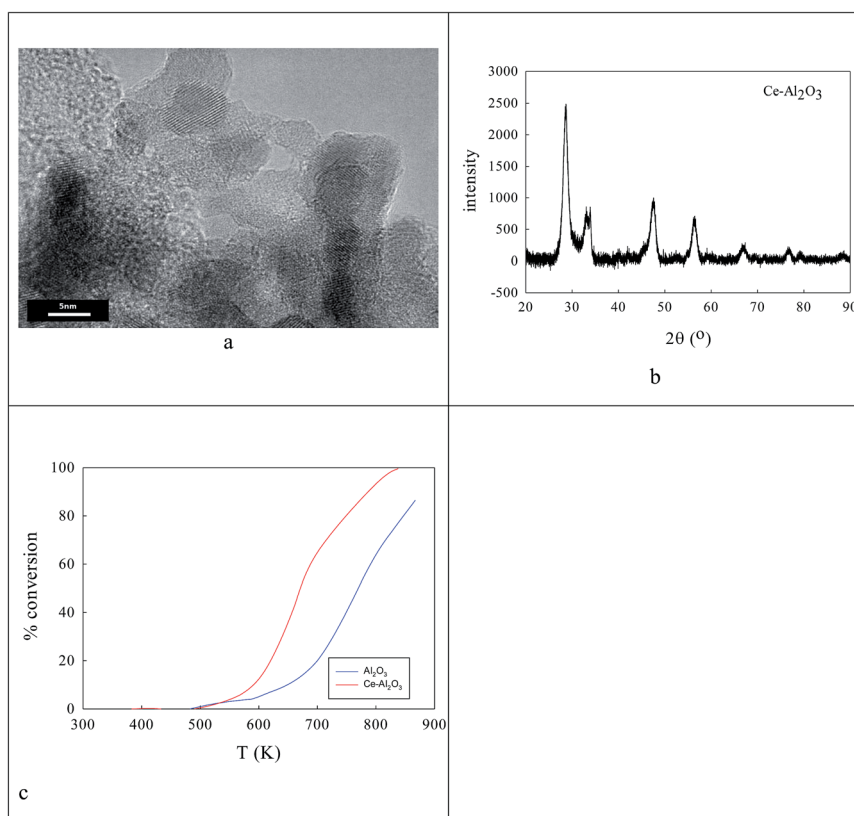
Fig. 3 Well-dispersed sol–gel 20% CeO_2–AlOOH (before calcination)/Al_2O_3 (after calcination) (168 m^2 g^{-1}) seen in (a) HRTEM and (b) XRD was slightly more active in CO oxidation under stoichiometric conditions (c) than the pure Al_2O_3 despite a 6.1% loss of surface area. HRTEM (a) shows 5 nm nano-crystallites (b). XRD (c) shows θ-Al_2O_3 and CeO_2 (but not CAO). H_2-TPR did, however, provide evidence in terms of a 900 K + β-peak for CAO.

Faraday Discussions

of the alumina support only, despite the loss of surface area, but there is no HC or NO conversion.

The ionic radius of Ba^{2+} (135 pm) is larger than that of Ce^{4+}. As the Ba^{2+} and Ce^{4+} contents inserted into the $AlOOH/Al_2O_3$ each rise from 0 to 25%, it was expected that $BaAl_2O_4$ would appear, that CeO_2 would segregate, but also that CAO or BCO might form in or at the surface of the host sol–gel matrix more strongly. It was found (see Fig. 4) that as the Ba,Ce content increased so HRTEM always showed 5–20 nm micro-domains of crystallinity (see Fig. 4a and b) and X-ray diffraction line broadening (XRDLB) (Fig. 4c) revealed unchanging and small average XRDLB crystallite sizes (d_{XRDLB}) while MASNMR saw 6-coordinate Al^{3+} gradually replaced by 4-coordinate (as $BaAl_2O_4$ appeared), XRD peak intensities
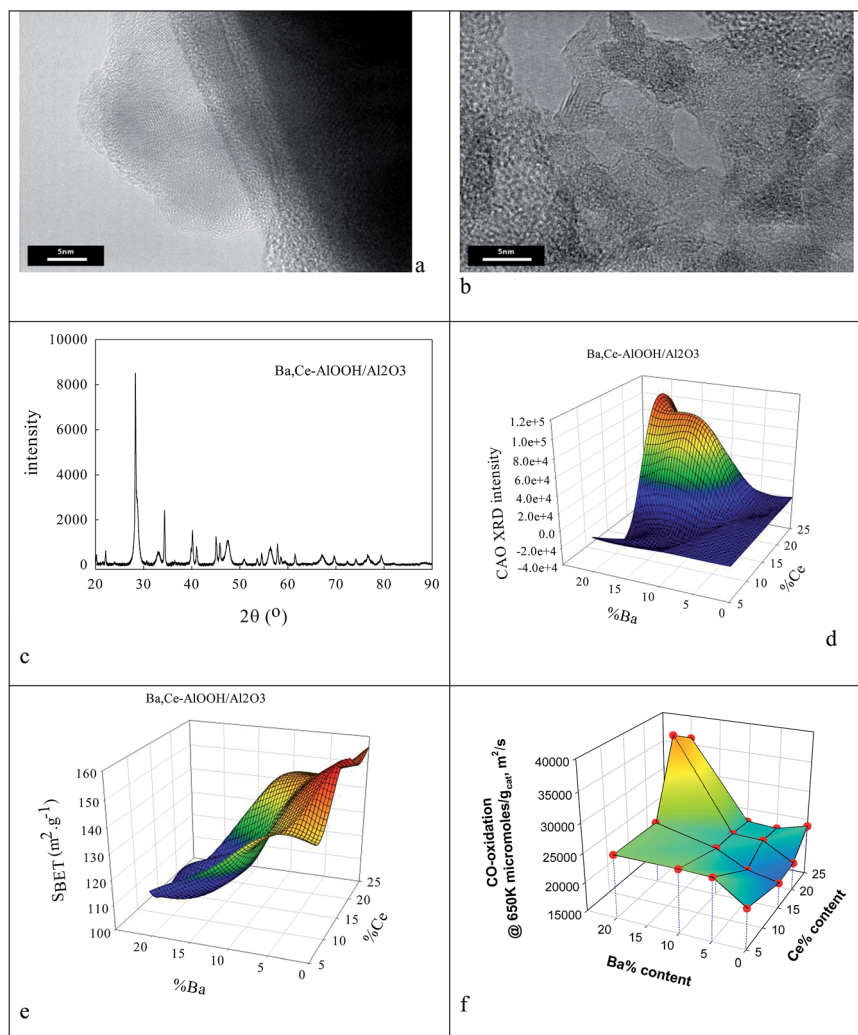

Fig. 4 Effect of Ba,Ce insertions at increasing levels into $AlOOH/Al_2O_3$ after calcination at 1223 K. HRTEM (a, b), XRD structure (c) and CAO level (d), surface area (e) and CO oxidation rate at 650 K in a stoichiometric reactant stream ($R = 1.13$) (f).

for $BaAl_2O_4$, CeO_2 and CAO (Fig. 4c and d) increased, surface areas decreased by 8% (Fig. 4e), and total CO (and propane, but not NO) conversion activity at 650 K increased (Fig. 4f).

To understand the nature of the highest CO oxidation catalytic activity (at high Ba,Ce addition levels) COT_O–OT_{CO} titrations of the surface were undertaken on 20% Ba,20% Ce–$AlOOH/Al_2O_3$ at 773 K and compared to EuroPt-1 at 573 K (see DSC profiles in Fig. 5 and integrated peak areas in Table 1) by DSC. Exothermic titration peaks increased in area or were stable with titration cycling, but the authors concentrated on the first CO titrations of surface $\underline{O}$ (COT_{O1}). On EuroPt-1 at 573 K ($COT_{O1} = 126.43$ J g^{-1}) COT_{O1} was 4.5× higher than for 88 m^2 g^{-1} 20% Ba,20% Ce–$AlOOH/Al_2O_3$ at 773 K ($COT_{O1} = 28.043$ J g^{-1}) and these were 57.2× higher than for 170 m^2 g^{-1} undoped-$AlOOH/Al_2O_3$ ($COT_{O1} = 0.490$ J g^{-1}) at 773 K. Interestingly, COT_{O1} can be converted to a number of active sites (*) adsorbing CO/g catalyst and hence to a turnover frequency (TOF); the TOF for 20% Ba,20% Ce–$AlOOH/Al_2O_3$ was 35% higher than for EuroPt-1 (see Table 1). Furthermore, the 20% Ba,20% Ce–$AlOOH/Al_2O_3$ showed a lower COT_O/OT_{CO} titration ratio than EuroPt-1 (suggesting less potential for CO poisoning). At high CeO_2 and BaO
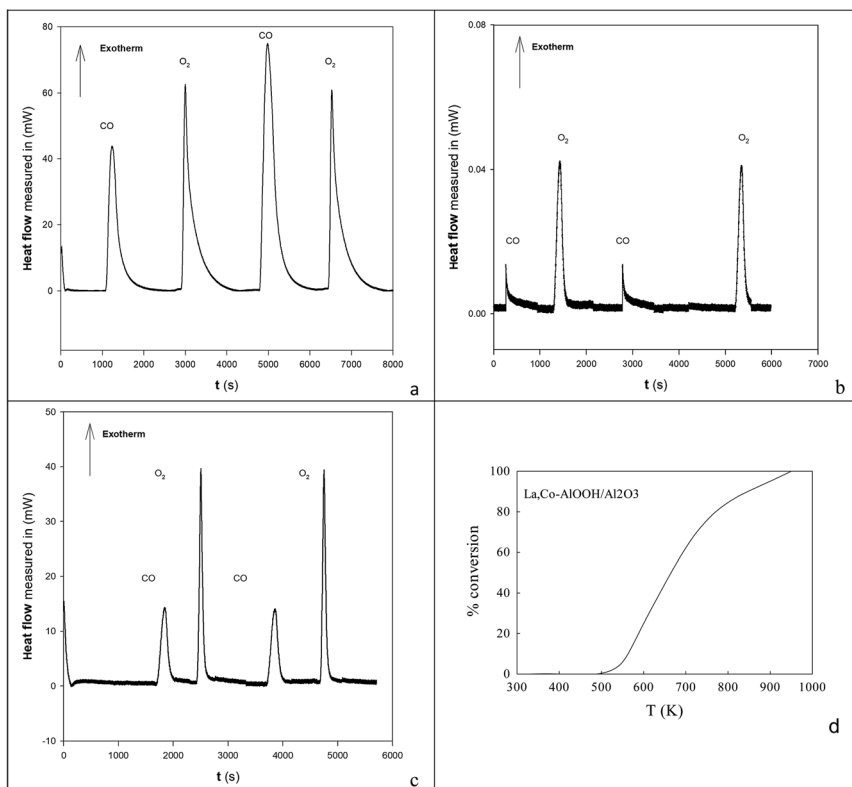
Fig. 5 DSC profiles for CO (40 µmol) and O_2 (47 µmol) titrations on (a) EuroPt-1 6.3% Pt/SiO_2 at 573 K (where $COT_{O1} = 126.43$ J g^{-1}; $OT_{CO1} = 182.37$ J g^{-1}); (b) $AlOOH/Al_2O_3$ (170 m^2 g^{-1}) at 773 K ($COT_{O1} = 0.490$ J g^{-1}) and (c) 20% Ba,20% Ce−$AlOOH/Al_2O_3$ at 773 K (88 m^2 g^{-1}) at 773 K ($COT_{O1} = 28.043$ J g^{-1}; $OT_{CO1} = 37.886$ J g^{-1}). (d) CO oxidation activity profile for 25% La,Co−$AlOOH/Al_2O_3$.
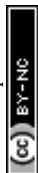
Table 1 Adsorption capacities, rates and TOFs for CO oxidation at 600 K under stoichiometric conditions (R = 1.13) for EuroPt-1 6.3% Pt/SiO$_2$ and 20% Ba,20% Ce–AlOOH/Al$_2$O$_3$ (calcined at 1223 K)

Catalysts	n_{CO} at[a] 773 K (μmol g$_{cat}^{-1}$)	Number of active sites (*)/g$_{cat}$ × 10^{-19}	Rate of CO oxidation[b] (molec per g$_{cat}$ per min)	TOF (molec per * per s)
EuroPt-1	57	3.4	4.1	0.20
20% Ba,20% Ce–AlOOH/Al$_2$O$_3$	41	2.5	4.1	0.27

[a] Monolayer CO capacity at 773 K. [b] At 600 K and R = 1.13.

concentrations, peaks from low concentrations of CAO and BCO (presumably at the interface between BaAl$_2$O$_4$ and CeO$_2$) appear in low concentration and may be significant contributors to catalytic activity.

La,Co doping was also achieved by replacing the 100 cm^3 water for AlOOH by a mixed metal nitrate aqueous solution. This was used to produce 25%La,Co–AlOOH/Al$_2$O$_3$. After calcination (923 K) this gave the catalytic profile in Fig. 5d, which is only slightly poorer than Fig. 2e. Hence both Ba,Ce and La,Co cation pairs can be inserted into AlOOH/Al$_2$O$_3$ and will produce activity in atmospheric pollution control reactions.

Surface complexation with pre-adsorbed oxalate to give 5% Ba,Ce– and 5% La,Co–AlOOH/Al$_2$O$_3$

Fig. 1c gave the average size of AlOOH dispersions seen in DLS (60 nm), on which oxalate anions were adsorbed,[85] followed by Ba,Ce or La,Co cations to form surface oxalates. Fig. 1d shows that this sequential coating caused the average particle size to rise to 114 nm after drying and calcination at 1223 K that was judged to be necessary to decompose oxalate species. Its oxidation activity was very modest (Fig. 6b).

TGA indicated that AlOOH lost 22% of its mass on heating, but this increased to 36% in 5% Ba,Ce–AlOOH/Al$_2$O$_3$ and 37% in 5% La,Co–AlOOH/Al$_2$O$_3$. XPS showed that the surface Ba : Ce surface atomic ratio was 25 : 75, while the La : Co XPS ratio on the surface was found to be 85 : 15. XPS-FAAS suggests these samples may be 0.91% Ba, 2.74% Ce–AlOOH/Al$_2$O$_3$ or 1.095% La,2.56% Co–AlOOH/Al$_2$O$_3$. Fig. 7a and b show that these samples contain micro-domains of crystallinity 3–5 nm in diameter. Thus XRD (a) and HRTEM (c, d) found 8–20 nm micro-domains of crystallinity. Analysis of HRTEM lattice images for Ba,Ce–AlOOH/Al$_2$O$_3$ (0.295 nm and 0.32 nm spacings) and La,Co–AlOOH/Al$_2$O$_3$ (0.225 nm and 0.296 nm spacings) gave line spacings after calcination greater than for AlOOH alone (0.19 nm; Fig. 6d). XRD of Ba,Ce–AlOOH/Al$_2$O$_3$ (Fig. 7e) shows that the dominant phase is probably 48.3 nm BaAl$_2$O$_4$, but there is also evidence from a (311) peak for 14.0 nm CeO$_2$ and traces of BCO and CeO$_2$/CAO. XRD for La,Co–AlOOH/Al$_2$O$_3$ (Fig. 7f) suggests that the dominant phases are 36–41.5 nm LAO and 17.68 nm Co$_3$O$_4$ but with LCO also present in small amounts. This ion preference may relate to oxalate insolubility, but would not help perovskite formation. CO and propane oxidation activity (Fig. 8a and b) was even lower than with sol–gel alumina (Fig. 3c).
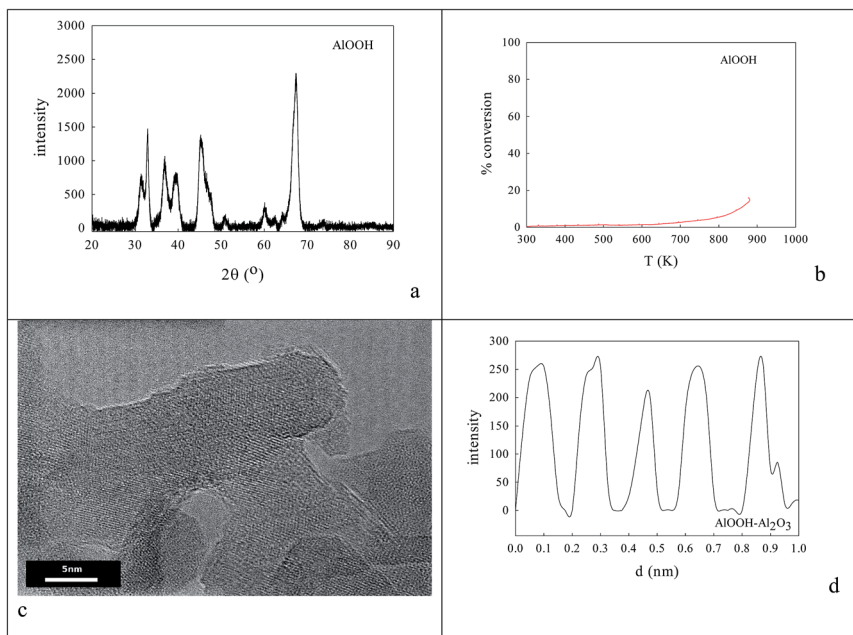
Fig. 6 AlOOH ($d_{DLS} = 60$ nm; see Fig. 2c)/Al_2O_3 samples onto which oxalate anions had been adsorbed,[84] then dried and calcined at 1223 K to decompose oxalate species, gave XRD (a) and HRTEM (c, d) evidence of 8–20 nm micro-domains of crystallinity. The most frequent XRD peaks appeared to be 11.70 nm θ-Al_2O_3 (with perhaps low levels of γ-Al_2O_3). The line spacing in micro-crystals was AlOOH (0.19 nm spacing), but activity in CO or propane oxidation or NO reduction (b) was even lower than with sol–gel alumina (Fig. 4f).

DSC measurements of the first COT_{O1} on EuroPt-1 at 423 K (ref. 58) was 143.01 kJ g^{-1} catalyst (2270 kJ g^{-1} Pt).[58] The summed heat flows in the first COT_{O1} from Ba,Ce/AlOOH (1.920 J g^{-1} catalyst) (and even more so La,Co/AlOOH (660.7 mJ g^{-1} catalyst)) (see Fig. 8c and d) were much smaller than those for EuroPt-1. That for COT_{O1} from Ba,Ce–AlOOH/Al_2O_3 (1.920 J g^{-1} catalyst) was a factor of 14 × lower than that for 20% Ba,20% Ce–AlOOH/Al_2O_3 sample (28.04 J g^{-1} catalyst), but that is not surprising given the imbalance of cations and the lower loading in the surface complexation samples.

4. Discussion and conclusions

It seems from the present work that microemulsion routes to BCO and LCO are effective and that the products adsorb on AlOOH sols, in much the same way as Turkevich immobilised platinum group metal sols.[1] BCO is active in CO and propane oxidation and NO removal under stoichiometric exhaust conditions, but LCO is a better oxidation catalyst. In calcination, the surfactant TX100 is removed, overcoming a frequent impurity disadvantage of μE routes.

Activity was also seen when Ba,Ce and La,Co are (i) inserted into AlOOH/Al_2O_3 and segregated at the surface, but in addition to formation of low levels of BCO, CAO, LCO and LAO perovskites, one also sees aluminates (e.g. $BaAl_2O_4$) and
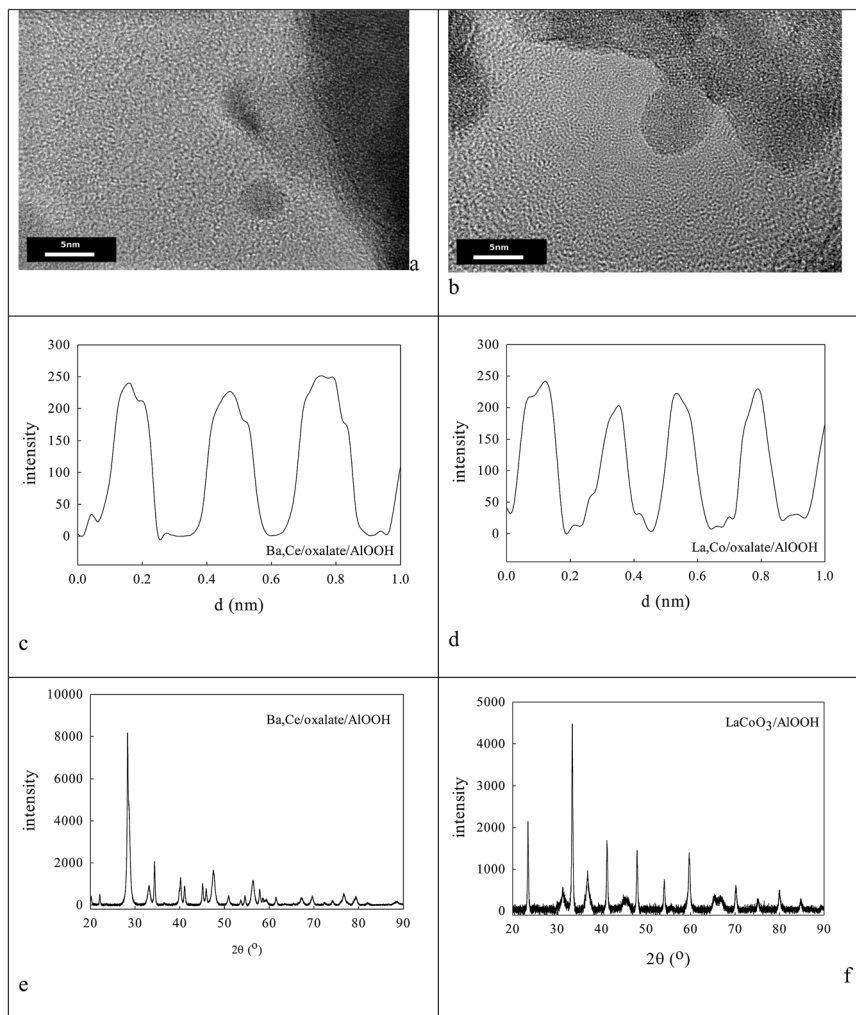
Faraday Discussions

Fig. 7 (a–d) HRTEM of Ba,Ce/oxalate/AlOOH (a, c) and La,Co/oxalate/AlOOH (b, d) produced from Ba^{2+} and Ce^{4+} cations adsorbed on oxalate/AlOOH, drying and then calcination at 1223 K. XRD of Ba,Ce/oxalate/AlOOH (e) and La,Co/oxalate/AlOOH (f) show the dominant and minor phases present.

separate oxide (*e.g.* CeO_2), although this might be minimised by fine tuning of cation loadings and (ii) when the cations were complexed with AlOOH surface-held oxalate ions, albeit with different efficiencies.

Therefore all three routes yield active catalysts with micro-domains of crystallinity.

The longer term aim of the present work was to design and produce nano-particulate perovskites, with a variety of cations,[46] stabilised by alumina (*i.e.* where there might be stabilisation by Al^{3+} substitution[47]). Of course one might still wish to use activation by Au nanoparticles/nanocrystals yielding green synergies[66] in catalysis[67] and gas sensing.[68]
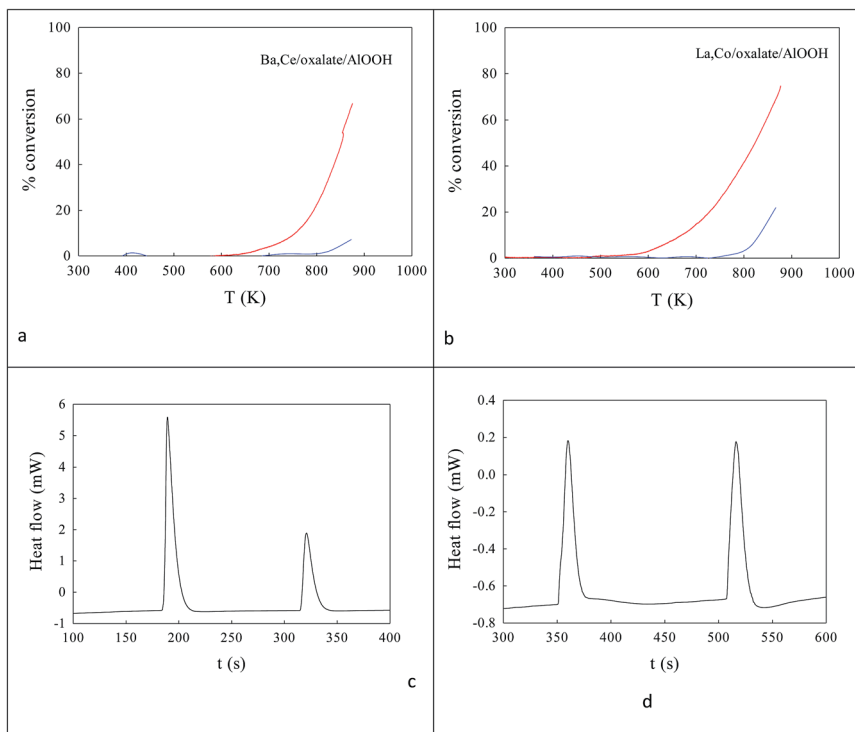
Fig. 8 Catalytic activities (a, b) and DSC analysis of COT_{O1} and OT_{CO1} titrations in flowing N_2 (c, d)[58] of Ba,Ce/oxalate/AlOOH (a, c) and La,Co/oxalate/AlOOH (b, d). Catalytic activities were modest for both these samples. The summed heat flows in the first COT_{O1} from Ba,Ce/oxalate/AlOOH (1.920 J g^{-1} catalyst) was a factor of 14× lower than that for the 20% Ba,20% Ce−AlOOH/Al$_2$O$_3$ sample (28.043 J g^{-1} catalyst) which is not surprising, given the lower loading in the surface complexation samples. COT_{O1} was even lower for La,Co/AlOOH (0.661 J g^{-1} catalyst).

Some have seen higher perovskite surface areas (*e.g.* LCO (22 m^2 g^{-1}) than LaMnO$_3$ (LMnO) (10 m^2 g^{-1})[13]). Some have compared the propane oxidation activity for 6–16 m^2 g^{-1} (S_{BET}) and 15–25 nm crystallite size ($d_{XRDLB-Scherrer}$) LMnO perovskites with 1% Pt/Al$_2$O$_3$ (ref. 89) and found that the temperatures of 10%, 50% and 90% oxidation ($T_{10\%}$, $T_{50\%}$ and $T_{90\%}$) were higher for the perovskites than the platinum group metal (PGM). The same authors found the perovskite-like trigonal X-ray diffraction patterns.[89] Others[90] have seen primary perovskite particle sizes, shapes, aggregation and structure by high resolution TEM. The present work should be seen against this background.

Here we have explored BaCeO$_3$ (BCO; that has been used in CO$_2$ conversion and characterised for structure by XRD[48] and embedded in hosts[49]) and LCO (that is useful in catalysed phenol removal from water[50]). We believe that the present routes offer an opportunity to develop green nanoparticle perovskite catalysts for a circular economy and a better environment, and that these might ultimately find use for other perovskite applications.[2]

Faraday Discussions

Acknowledgements

Notes and references

1 J. Turkevich and G. Kim, *Science*, 1970, **169**, 873–879; K. Aika, L. L. Ban, I. Okura, S. Namba and J. Turkevich, *J. Res. Inst. Catal., Hokkaido Univ.*, 1976, **25**, 54–64; J. Turkevich, *Gold Bull.*, 1985, **18**(4), 125–131.

2 R. J. D. Tilley, *Perovskites: structure-property relationships*, 2016, Wiley.

3 S. R. Noh, D. Lee, S. J. Park, D. S. Kim and M. Choi, *Aerosol Sci. Technol.*, 2017, **51**, 116–122.

4 V. Solanki, S. Das, S. Kumar, M. M. Seikh, B. Raveaun and A. K. Kundu, *J. Sol-Gel Sci. Technol.*, 2017, **82**, 536–540.

5 N. Bhardwaj, A. Gaur and K. Yadav, *Appl. Phys. A: Mater. Sci. Process.*, 2017, **123**, 429.

6 S. D. Li, Z. X. He, X. L. Wang and K. Gao, *Appl. Phys. A: Mater. Sci. Process.*, 2014, **117**, 1381–1386.

7 S. Ifrah, A. Kaddouri, P. Gelin and D. Leonard, *C. R. Chim.*, 2007, **10**, 1216–1226.

8 S. A. E. Abdulla, P. A. Sermon, M. Worsley and I. R. Collins, Nanostructured Mater. Nanotechnol. IV, *Ceram. Eng. Sci. Proc.*, 2008, **28**, 131.

9 L. M. Chao, Y. D. Hou, M. P. Zheng, Y. G. Yue and M. K. Zhu, *J. Alloys Compd.*, 2017, **695**, 3331–3338.

10 M. Yousefi and M. Ranjbar, *J. Inorg. Organomet. Polym. Mater.*, 2017, **27**, 633–640.

11 T. Tabari, D. Singh, A. Calisan, M. Ebadi, H. Tavakkoli and B. Caglar, *Ceram. Int.*, 2017, **43**, 15970–15977.

12 M. M. Hessien, G. A. M. Mersal, Q. Mohsen and D. Alosaimi, *J. Mater. Sci.: Mater. Electron.*, 2017, **28**, 4170–4178.

13 E. Krupicka, A. Reller and A. Weidenkaff, *Cryst. Eng.*, 2002, **5**, 195–202.

14 R. N. Das and P. Pramanik, *Mater. Lett.*, 2000, **46**, 7–14.

15 S. A. Kulkarni, S. Muduli, G. C. Xing, N. Yantara, M. J. Li, S. Chen, T. C. Sum, N. Mathews, T. J. White and S. G. Mhaisalkar, *ChemSusChem*, 2017, **10**, 3818–3824.

16 M. E. F. Bouduban, A. Burgos-Caminal, R. Ossola, J. Teuscher and J. E. Moser, *Chem. Sci.*, 2017, **8**, 4371–4380.

17 G. Kakavelakis, K. Petridis and E. Kymakis, *J. Mater. Chem. A*, 2017, **5**, 21604–21624.

18 Y. H. Kim, G. H. Lee, Y. T. Kim, C. Wolf, H. J. Yun, W. Kwon, C. G. Park and T. W. Lee, *Nano Energy*, 2017, **38**, 51–58.

19 R. Zhou, Y. Z. Huang, L. Wan, H. H. Niu, F. W. Ji and J. Z. Xu, *J. Alloys Compd.*, 2017, **716**, 162–170.

20 L. Durai, B. Moorthy, C. I. Thomas, D. K. Kim and K. K. Bharathi, *Mater. Sci. Semicond. Process.*, 2017, **68**, 165–171.

21 L. T. Ye, M. Y. Zhang, P. Huang, G. C. Guo, M. C. Hong, C. S. Li, J. T. S. Irvine and K. Xie, *Nat. Commun.*, 2017, **8**, 14785.
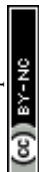
22 N. Afifah and R. Saleh, Internat. Conf. Eng. Sci. Nanotechnol. (ICESNANO 2016), *AIP Conf. Proc.*, 2017, **1788**, 030080.

23 H. Wang, Z. Zhao, C. M. Xu, J. Liu and Z. X. Lu, *Chin. Sci. Bull.*, 2005, **50**, 1440–1444.

24 Y. Zhang-Steenwinkel, L. M. van der Zande, H. L. Castricum, A. Bliek, R. W. van den Brink and G. D. Elzinga, *Chem. Eng. Sci.*, 2005, **60**, 797–804.

25 T. Maneerung, K. Hidajat and S. Kawi Internat, *Int. J. Hydrogen Energy*, 2017, **42**, 9840–9857.

26 M. J. Suh, Y. K. Park and S. K. Ihm, *Catal. Today*, 2016, **265**, 210–217.

27 S. S. Li, H. G. Tang, D. D. Gong, Z. Ma and Y. Liu, *Catal. Today*, 2017, **297**, 298–307.

28 H. Einaga, Y. Nasu, M. Oda and H. Saito, *Chem. Eng. J.*, 2016, **283**, 97–104.

29 A. Lay-Ekuakille, S. Ikezawa, M. Mugnaini, R. Morello and C. De Capua, *Measurement*, 2017, **98**, 49–59.

30 Y. Zhang-Steenwinkel, H. L. Castricum, A. Bliek and E. Esveld, *J. Mater. Sci.*, 2007, **42**, 5851–5859.

31 H. L. T. N'Goc, L. D. N. Mouafo, C. Etrillard, A. Torres-Pardo, J. F. Dayen, S. Rano, G. Rousse, C. Laberty-Robert, J. G. Calbet, M. Drillon, C. Sanchez, B. Doudin and D. Portehault, *Adv. Mater.*, 2017, **29**, 1604745.

32 W. Zhang, X. D. Zuo, Y. Niu, C. W. Wu, S. P. Wang, S. Guan and S. R. P. Silva, *Nanoscale*, 2017, **9**, 13929–13937.

33 C. O. Ehi-Eromosele, B. I. Ita and E. E. J. Iweala, *Colloids Surf., A*, 2017, **530**, 164–171.

34 Q. W. Shen, Y. D. Zhang, H. R. Ding, L. J. Wu, Y. Q. Xu, B. C. Shi, Y. Zheng and J. L. Yuan, *Energies*, 2017, **10**, 164.

35 Y. C. Ye, H. Yang, R. S. Li and X. X. Wang, *J. Sol-Gel Sci. Technol.*, 2017, **82**, 509–518.

36 S. S. Li, H. G. Tang, D. D. Gong, Z. Ma and Y. Liu, *Catal. Today*, 2017, **297**, 298–307.

37 Y. Janbutrach, S. Hunpratub and E. Swatsitang, *Nanoscale Res. Lett.*, 2014, **9**, 498.

38 D. G. Shchukin, A. A. Yaremchenko, M. G. S. Ferreira and V. V. Kharton, *Chem. Mater.*, 2005, **17**, 5124–5129.

39 R. A. Sheldon, *Green Chem.*, 2016, **18**, 3180–3183.

40 E. Grabowska, *Appl. Catal., B*, 2016, **186**, 97–126.

41 W. F. Libby, *Science*, 1971, **171**(3970), 499–500.

42 K. A. Grant, K. M. Keryou and P. A. Sermon, *Faraday Discuss.*, 2008, **138**, 257–271.

43 M. R. Soames, PhD thesis, Brunel University, 2000.

44 P. Klonowski, J. C. Goloboy, F. J. Uribe-Romo, F. R. Sun, L. Y. Zhu, F. Gandara, C. Wills, R. J. Errington, O. M. Yaghi and W. G. Klemperer, *Inorg. Chem.*, 2014, **53**, 13239–13246.

45 C. Thatcher, PhD thesis, University of Surrey, 2005.

46 M. V. Goldschmidt, *Naturwissenschaften*, 1926, **14**(21), 477–485.

47 Z. R. Ismagilov, R. A. Shkrabina, N. A. Koryabkina and F. Kapteijn, *Catal. Today*, 1995, **24**, 269–271; R. A. Shkrabina, N. A. Koryabkina, O. A. Kirichenko, V. A. Ushakov, F. Kapteijn and Z. R. Ismagilov, *Stud. Surf. Sci. Catal.*, 1995, **91**, 1145–1152.

48 S. Cimino, L. Lisi, S. De Rossi, M. Faticanti and P. Porta, *Appl. Catal., B*, 2003, **43**, 397–406.

49 I. Pettiti, S. Colonna, S. De Rossi, M. Faticanti, G. Minelli and P. Porta, *Phys. Chem. Chem. Phys.*, 2004, **6**, 1350–1358.

50 M. A. Malecka and L. Kepinski, *CrystEngComm*, 2015, **17**, 2273–2278; M. A. Malecka and L. Kepinski, *CrystEngComm*, 2015, **17**, 8282–8288.

51 A. Piras, S. Colussi, A. Trovarelli, V. Sergo, J. Llorca, R. Psaro and L. Sordelli, *J. Phys. Chem. B*, 2005, **109**, 11110–11118.

52 S. I. Lopatin, S. M. Shugurov, A. V. Fedorova, A. V. Utina and A. I. Panin, *J. Alloys Compd.*, 2017, **693**, 1028–1034.

53 JCPDS 22-74; 15–148.

54 L. Tepech-Carrillo, A. Escobedo-Morales, A. Perez-Centeno, E. Chigo-Anota, J. F. Sanchez-Ramirez, E. Lopez-Apreza and J. Gutierrez-Gutierrez, *J. Nanomater.*, 2016, 6917950.

55 D. P. Belanger, T. Keiber, F. Bridges, A. M. Durand, A. Mehta, H. Zheng, J. F. Mitchell and V. Borzenets, *J. Phys.: Condens. Matter*, 2016, **28**, 025602.

56 JCPDS 9–358.

57 G. J. Liu, X. T. Li, Y. Q. Wang, W. S. Liang, B. Liu, H. L. Feng, H. W. Yang, J. Zhang and J. R. Sun, *Appl. Surf. Sci.*, 2017, **425**, 121–129.

58 M. A. M. Luengo, P. A. Sermon and A. T. Wurie, *J. Chem. Soc., Faraday Trans. 1*, 1987, **83**, 1651–1665.

59 S. Roesch, P. A. Sermon, A. Wallum, P. N. Forrest and P. Kaur, *Top. Catal.*, 2001, **16**, 115–118; T. Salvesen, S. Roesch, P. A. Sermon and P. Kaur, *Top. Catal.*, 2001, **16**, 381–384.

60 J. Z. Shyu, W. H. Weber and H. S. Gandhi, *J. Phys. Chem.*, 1988, **92**, 4964–4970.

61 C. Morterra, V. Bolis and G. Magnacca, *J. Chem. Soc., Faraday Trans.*, 1996, **92**, 1991–1999.

62 B. Harrison, A. F. Diwell and C. Hallett, *Platinum Met. Rev.*, 1988, **32**, 73.

63 A. F. Diwell, R. R. Rajaram, H. A. Shaw and T. J. Truex, *Stud. Surf. Sci. Catal.*, 1991, **71**, 139–152.

64 L. Matějová, P. Topka, L. Kaluža, S. Pitkäaho, S. Ojala, J. Gaálová and R. L. Keiski, *Appl. Catal., B*, 2013, **142–143**, 54–64.

65 S. K. Saji, R. Vinodkumar, S. M. Eappen and P. R. S. Wariar, *Mater. Chem. Phys.*, 2017, **193**, 189–195.

66 A. M. Harzandi, J. N. Tiwari, H. S. Lee, H. Jeon, W. J. Cho, G. Lee, J. Baik, J. H. Kwak and K. S. Kim, *ACS Appl. Mater. Interfaces*, 2017, **9**, 2495–2499.

67 P. Ciambelli, S. Cimino, G. Lasorella, L. Lisi, S. De Rossi, M. Faticanti, G. Minelli and P. Porta, *Appl. Catal., B*, 2002, **37**, 231–241.

68 S. Cimino, L. Lisi, S. De Rossi, M. Faticanti and P. Porta, *Appl. Catal., B*, 2003, **43**, 397–406.

69 H. H. Wang, L. L. Zhang, C. Hu, X. K. Wang, L. Lyu and G. D. Sheng, *Chem. Eng. J.*, 2018, **332**, 572–581.

70 L. Q. Wang, Q. Pang, Q. Q. Song, X. W. Pan and L. S. Jia, *Fuel*, 2015, **140**, 267–274.

71 M. M. Natile, G. Eger, P. Batocchi, F. Mauuy and A. Glisenti, *Int. J. Hydrogen Energy*, 2017, **42**, 1724–1735.

72 D. Y. Yoon, Y. J. Kim, J. H. Lim, B. K. Cho, S. B. Hong, I. S. Nam and J. W. Choung, *J. Catal.*, 2015, **330**, 71–83.
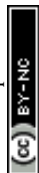
73 L. F. Liotta, G. Di Carlo, A. Longo, G. Pantaleo, G. Deganello, G. Marci and A. Martorana, *J. Non-Cryst. Solids*, 2004, **345**, 620–623.

74 G. Lee, I. Kim, I. Yang, J. M. Ha, H. B. Na and J. C. Jung, *Appl. Surf. Sci.*, 2018, **429**, 55–61.

75 H. M. Zhang, R. S. Hu, J. N. Hu and Y. L. Zhang, *Acta Phys.-Chim. Sin.*, 2011, **27**, 1169–1175.

76 J. Cai, K. Laubernds, F. S. Galasso, S. L. Suib, J. Liu, X. F. Shen, E. Begge, H. R. Kunz and J. M. Fenton, *J. Am. Ceram. Soc.*, 2005, **88**, 2729–2735.

77 P. Fornasiero, G. Balducci, J. Kaspar, S. Meriani, R. diMonte and M. Graziani, *Catal. Today*, 1996, **29**, 47–52.

78 K. Masuda, T. Sano, F. Mizukami and M. Watanabe, *Catal. Lett.*, 1995, **33**, 229–235.

79 B. E. Yoldas, *Am. Ceram. Soc. Bull.*, 1975, **54**, 286–290; B. E. Yoldas, *J. Mater. Sci.*, 1975, **10**, 1856–1857.

80 T. Maunula, Y. Kintaichi, M. Haneda and H. Hamada, *Catal. Lett.*, 1999, **61**, 121–130.

81 K. Maeda, F. Mizukami, M. Watanabe, N. Arai, S. Nniwa, M. Toba and K. Shimizu, *J. Mater. Sci. Lett.*, 1990, **9**, 522–523.

82 K. Maeda, F. Mizukami, S. Niaw, M. Toba, M. Watanabe and K. Masuda, *J. Chem. Soc., Faraday Trans.*, 1992, **88**, 97–104.

83 N. E. Bogdanchikova, S. Fuentes, M. Avalos-Borja, M. H. Farias, A. Boronin and G. Diaz, *Appl. Catal., B*, 1998, **17**, 221–231.

84 M. J. D' Aniello, *J. Catal.*, 1981, **69**, 9–17.

85 M. F. L. Johnson and J. Mooi, *J. Catal.*, 1987, **103**, 502–505.

86 E. Rogemond, R. Frety, V. Perrichon, M. Primet, S. Salasc, M. Chevrier, C. Gauthier and F. Mathis, *J. Catal.*, 1997, **169**, 120–131.

87 J. Z. Shyu, K. Otto, W. L. H. Watkins, G. W. Graham, R. K. Belitz and H. S. Gandhi, *J. Catal.*, 1988, **114**, 23–33.

88 J. Wang, C. X. Huang, X. L. Chen, H. T. Zhang, Z. S. Li and Z. G. Zou, *Appl. Surf. Sci.*, 2015, **358**, 463–467.

89 N. Miniajluk, J. Trawczynski and M. Zawadzki, *Appl. Catal., A*, 2017, **531**, 119–128.

90 M. Ogasawara, S. Kato, H. Tsukidate, T. Akaogi, Y. Moriya and S. Nakata, *Chem. Lett.*, 2005, **34**, 208–209.